Journal of Materials Chemistry A

ROYAL SOCIETY OF CHEMISTRY

PAPER

View Article Online
View Journal | View Issue

Cite this: J. Mater. Chem. A, 2026, 14, 12003

Cyclic olefin copolymer-based reinforced anion exchange membranes for water electrolyzers

Heemin Park, [a] Jong Yeob Jeon,[a] Pothana Gandhi Nellepalli,[a] Ju Yeon Lee,[a] Daniel Philip Leonard, [b] Sun Young Kang, [b] Yu Seung Kim *[b] and Chulsung Bae *[a]

Anion exchange membranes (AEMs) have emerged as a promising technology for water electrolysis in hydrogen production since they offer significant cost reduction in choices of electrocatalysts and bipolar plates. However, AEMs satisfying multiple requirements of high ionic conductivity, good chemical stability, robust mechanical properties, scalable synthesis, and low manufacturing costs are rare. Herein, we introduce quaternary ammonium functionalized cyclic olefin copolymers (COCs) as a new class of chemically stable and low-cost AEM materials. To further enhance the mechanical robustness, we prepared reinforced composite AEMs by impregnating the ionically functionalized COC into a mechanically robust matrix. The resulting reinforced composite membrane exhibits a high hydroxide conductivity of 127 mS cm^{-1} and excellent mechanical strength. In water electrolyzers, the MEA demonstrated outstanding performance, achieving a current density of 2.24 A cm^{-2} at 1.8 V, attributable to high conductivity, enhanced mechanical properties, and good alkaline stability of the composite membrane. These results indicate that the COC-based AEMs demonstrate good potential for application in AEM electrolyzers.

Received 3rd November 2025
Accepted 30th January 2026

DOI: 10.1039/d5ta08898d

rsc.li/materials-a

1. Introduction

Hydrogen technologies, particularly water electrolysis systems, provide a promising pathway for the efficient and cost-effective hydrogen production from renewable energy sources.[1–3] Anion exchange membrane (AEM) water electrolyzers represent a promising technology that combines advantages of both liquid alkaline electrolyzers and proton exchange membrane (PEM) water electrolyzers. AEM water electrolyzers operate in alkaline environments and use an alkaline membrane (*i.e.*, the AEM) to transport OH^- ions across the electrodes.[4,5] They can also utilize nonprecious metals, such as nickel or iron, as electrocatalysts and stainless steel bipolar plates while PEM water electrolyzers require precious metal catalysts and titanium bipolar plates.[6,7] Despite these advantages, the full potential of AEM electrolyzers has not been materialized, in part due to the lack of low-cost, easily scalable, durable, high performance AEM materials that can serve as a standard AEM.[7–9]

AEMs, which typically contain positively charged cationic groups attached to a polymer backbone, function as solid hydroxide ion conductors, and they are key components of AEM electrochemical devices.[2] Until the mid-2010s, polysulfone, poly(ether ketone), and poly(aryl ether) were commonly used as the polymeric backbone choice of anion exchange polymers of AEMs because of their good thermal and mechanical properties. However, aryl ether (Csp_2–O) bonds of these aromatic polymers can be cleaved by nucleophilic attack of hydroxide, especially when aryl groups are activated by electron-withdrawing groups such as a quaternary ammonium or sulfone. The chemical and alkaline stability of AEMs under high pH conditions can be greatly improved by removing labile aryl ether bonds from chemical structures of polymers and substituting them with C–C bonds in the polymer backbone.[2,10–12] For example, researchers have demonstrated good alkaline stability of AEMs when their backbones are composed of all C–C bonds, which include poly(phenylene alkylene)s,[13–16] polypropylene,[17,18] SEBS,[19,20] and polynorbornene AEMs.[21–23]

Polynorbornene is an attractive polymer backbone choice for AEM applications and has been investigated by several research groups. Noonan *et al.*[24] synthesized polynorbornene AEMs from vinyl addition polymerization of 5-*n*-hexyl-2-norbornene and 5-(4-bromobutyl)-2-norbornene. The optimized AEM with an IEC of 1.91 mmol g^{-1} showed a hydroxide conductivity of 95 mS cm^{-1} at 80 °C. Kohl *et al.*[25] reported synthesis of cross-linked AEMs using ring-opening metathesis polymerization of norbornene monomers and the optimized membrane (XL20-rPNB-LY100) demonstrated a conductivity of 195 mS cm^{-1} (at 80 °C) and no chemical degradation after 792 hours in 1 M NaOH at 80

[a]Department of Chemistry and Chemical Biology, Rensselaer Polytechnic Institute, Troy, NY 12180, USA. E-mail: baec@rpi.edu

[b]MPA-11: Materials Synthesis and Integrated Devices, Los Alamos National Laboratory, Los Alamos, New Mexico 87545, USA. E-mail: yskim@lanl.gov

°C. Wei *et al.*[26] synthesized an AEM based on polycyclic norbornene derivatives from dicyclopentadiene and tricyclopentadiene.

There are two synthetic methods for preparation of polynorbornenes and they yield quite different materials and properties. Polynorbornene prepared by ring-opening metathesis polymerization generates an amorphous polymer with a low glass transition temperature (T_g) of around 35 °C and it requires follow-up hydrogenation to remove C=C bonds in the polymer backbone.[27–29] In contrast, addition-type polymerization of norbornene yields polynorbornenes with good thermo-mechanical properties without the presence of C=C bonds in the polymer backbone. However, addition-type polynorbornenes tend to be brittle.[25,28,30] Copolymerization of ethylene and norbornene, typically conducted using metallocene catalysts such as zirconocene or half-sandwich titanium/MAO catalysts, affords cyclic olefin copolymers (COCs) which can resolve this issue. In COC synthesis, the highly active metallocene catalysts generate polymers with high molecular weights which is very important for delivery of good mechanical properties.[31,32]

For AEMs to be used in electrochemical devices, AEM materials should simultaneously fulfil numerous essential characteristics, which include high ionic conductivity, low area specific resistance (ASR), robust chemical stability at high pH and temperature (>80 °C), and tough mechanical properties. Scalability and manufacturing cost of polymers are also critically important criteria for broad adoption of AEMs in electrochemical technologies, but they are often not discussed in the literature. In this regard, polyolefins such as COCs are attractive candidates for AEM materials as it is well demonstrated that they can be manufactured on large scales at low cost without using complicated synthetic procedures.[33] In the case of COCs, thermal and mechanical properties can be easily tuned to meet specific applications by adjusting the ratio of ethylene and norbornene in polymerization; as more norbornene units are incorporated, it yields COCs with higher T_g and higher tensile strength. Commercially, COCs are widely used as packaging and optical component materials due to their good mechanical properties, high optical transparency, and excellent chemical resistance. However, the incorporation of a polar functional group into polyolefin is quite challenging because metallocene catalysts and Ziegler–Natta catalysts, which are commonly used in polyolefin synthesis, are easily poisoned by the lone pair electrons of polar functionality in polymerization.

Herein, we introduce quaternary ammonium (QA) functionalized COCs as a new class of high-performance, alkaline-stable, low-cost AEM materials. In addition, we prepared reinforced composite AEMs by pore-filling the functionalized COC into a mechanically robust porous polyethylene substrate. The reinforced COC membranes result in high hydroxide conductivity, good dimensional stability, alkaline stability, and enhanced mechanical properties and demonstrate good performance in water electrolyzers when they are used as an AEM. While our COC AEMs are synthesized *via* addition polymerization of norbornene, they are distinctly different from traditional polynorbornene AEMs in terms of their polymerization chemistry and the mechanisms used to tune their mechanical properties. The addition-type polymerization of norbornene uses a late transition metal catalyst (mostly the Pd catalyst)[21–26] and requires non-functionalized alkyl sidechain-substituted (*e.g.*, *n*-C_6H_{13}–) norbornene as a comonomer to tune mechanical properties and enhance solubility of the polymers. In contrast, the polymerization of COCs uses a typical metallocene olefin polymerization catalyst (*e.g.*, zirconocene and MAO co-catalysts) which is several orders of magnitude more reactive than the Pd catalyst used in the addition-type polymerization of norbornene. The COC is a copolymer of ethylene, the most reactive olefin in polymerization; the major component in the COC repeating unit is ethylene and the norbornene unit is a minor component. Mechanical properties are controllable by adjusting the ratio of ethylene and norbornene units in COC repeating units.

2. Results and discussion

2.1 Synthesis of functionalized COCs

Fig. 1 shows the synthesis route of functionalized COCs that are used as AEMs in this study. The monomer PhNB was conveniently synthesized by the Diels–Alder reaction of dicyclopentadiene and styrene. Fig. 2(a) shows the ^{1}H NMR spectrum of PhNB. The NMR data confirmed that PhNB is composed of 80% endo-phenyl norbornene and 20% exo-phenyl norbornene isomers. The chemical shifts at 6.8–7.2 ppm (peak a) were assigned to the 5 protons of the aromatic ring while peaks b–g confirm the attachment of a phenyl ring to the norbornene unit. COC-Ph was prepared by copolymerization of PhNB and ethylene under inert conditions. The ethylene unit provides flexibility to the resulting copolymer, while the PhNB unit gives rigidity. The PhNB incorporation ratio in the

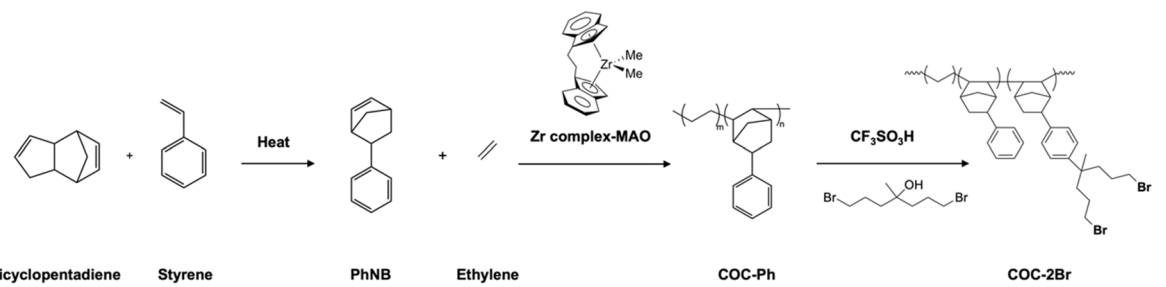

Fig. 1 Synthetic route for cyclic olefin copolymers and their bromoalkyl functionalization.

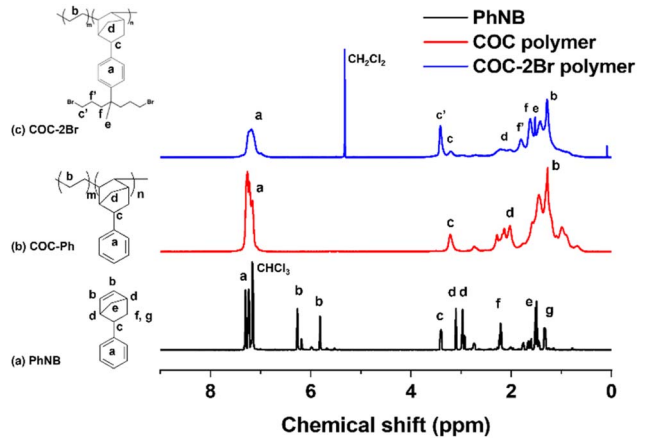

Fig. 2 ^{1}H NMR spectra (in $CDCl_3$, 500 MHz) of (a) PhNB monomer, (b) COC-Ph polymer, and (c) dibromoalkylated polymer COC-2Br.

copolymer (*i.e.*, $n/(m+n)$ in COC-Ph) could be controlled from 16 to 45 mol% by changing the feed ratio of the two monomers. Glass transition temperature (T_g) of COC-Ph increases as PhNB content of the copolymer increases. A metallocene catalyst [(EBI)$ZrCl_2$] was used for the polymerization of PhNB and ethylene, and it was activated using the modified methylaluminoxane (MAO) co-catalyst. The catalytic activity was ~3.0 × 10^6 g mol^{-1} Zr h. As expected, the metallocene catalyst afforded COC-Ph with high molecular weights. For example, weight average molecular weight (M_w) of COC-2Br with $n/(m+n)$ = 34 mol% and Br content = 2.2 mmol g^{-1} was 733 000 g mol^{-1}.

Once COC-Ph was prepared, its aromatic rings were functionalized by Friedel–Crafts alkylation using 1,7-dibromo-4-methylheptan-4-ol and triflic acid. The degree of functionalization in the alkylation can be controlled by adjusting the amount of 1,7-dibromo-4-methylheptan-4-ol relative to the phenyl group in COC-Ph and was calculated from ^{1}H NMR data (Fig. 2(c)) by comparing the integral ratio of the phenyl aromatic protons (4H, peak a) with the combined signal of the norbornene bridge proton (1H, peak c) and the two methylene protons (4H, peak c′) attached to Br at the end, which appear at 3.42 and 3.19 ppm, respectively. For example, COC–2Br with 38% degree of functionalization was obtained when 1.4 equivalents of 1,7-dibromo-4-methylheptan-4-ol were added relative to the phenyl group. A summary of polymer functionalization and molecular weight information of COC–2Br alkylation reactions is listed in Table S1.

2.2 Properties of non-reinforced COC membranes and pore-filled reinforced membranes

As summarized in Table 1, membrane properties of COC AEMs were studied by measuring ion exchange capacity (IEC), water uptake, swelling ratio in water, and hydroxide conductivity. The IEC values were obtained from Mohr titration and analysis of the ^{1}H NMR spectrum. For reinforced COC membranes in Table 1, the NMR IEC represents IEC of the QA-functionalized COC (non-reinforced) from the ^{1}H NMR spectrum while the titration IEC represents IEC of polyethylene (PE)-supported reinforced membranes of the corresponding COCs by titration. As expected, the titration IECs of reinforced membranes are slightly lower than the calculated IEC from NMR due to the additional mass of the PE substrate in reinforced membranes. As IEC values increase, water uptake and swelling ratio values of the membranes increase accordingly. For comparison with the reinforced membranes, the properties of non-reinforced membrane XL20-COC-2N-2.1 are included in entry (a) in Table 1. It showed a significantly higher swelling ratio compared with reinforced membranes with a similar IEC range (25% swelling ratio for XL20-COC-2N-2.1 *vs.* an 8% swelling ratio for R-XL-20-COC-2N-2.2-PE; entry (b) in Table 1). Even reinforced membranes with higher IECs demonstrated exceptionally good dimensional stability in length and width directions due to the non-swellable nature of the PE substrate.

High hydroxide conductivity is essential for achieving good performance in AEM electrolyzers. As anticipated, in-plane hydroxide conductivity of all membranes increased with the rise in temperature. Notably, the R-XL20-COC-2N-2.2-PE and R-XL20-COC-2N-2.3-PE reinforced membranes exhibited high hydroxide ion conductivity greater than 100 mS cm^{-1} at 80 °C. However, the self-supporting membrane XL20-COC-2N-2.1 which has a lower IEC was more conductive than the reinforced membranes. To confirm this behaviour, we calculated activation energy of the membranes. The temperature dependence of conductivity, which follows the linear Arrhenius behaviour (Fig. 3), allows activation energies (E_a) to be extracted from the corresponding Arrhenius plots. Thus, activation

Table 1 Properties of non-reinforced and pore-filled reinforced COC AEMs

Entry	Membrane[a]	Calculated IEC from ^{1}H NMR (mequiv. g^{-1})	Titration IEC (mequiv. g^{-1})	Water uptake (%, OH^-)	Swelling ratio (%, OH^-)	OH^- conductivity (mS cm^{-1})		
						30 °C	60 °C	80 °C
(a)	XL20-COC-2N-2.1	2.1	2.1 ± 0.01	76 ± 3	25 ± 0	67 ± 6	111 ± 4	134 ± 0
(b)	R-XL20-COC-2N-2.2-PE	2.4	2.2 ± 0.1	62 ± 2	8 ± 1	46 ± 9	79 ± 18	127 ± 6
(c)	R-XL20-COC-2N-2.3-PE	2.5	2.3 ± 0.1	67 ± 3	10 ± 1	52 ± 3	85 ± 11	123 ± 1
(d)	R-XL20-COC-2N-2.5-PE	2.7	2.5 ± 0.0	73 ± 10	11 ± 2	–[b]	–[b]	–[b]
(e)	R-XL20-COC-2N-2.8-PE	3.0	2.8 ± 0.1	96 ± 0	14 ± 0	–[b]	–[b]	–[b]

[a] R: reinforced membrane, XL20: 20% crosslinking density, 2N-xx: two QA groups per functionalized COC-Ph unit and xx IEC value, and PE: polyethylene-supported AEM. [b] Not measured due to extensive curling behaviour.

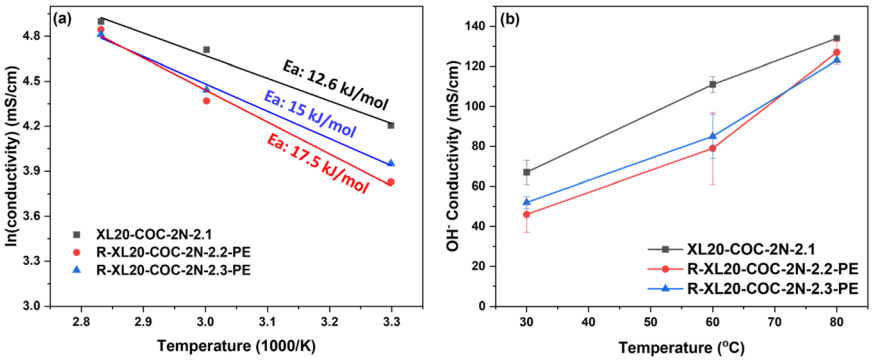

Fig. 3 (a) Hydroxide conductivity for non-reinforced and pore-filled reinforced COC AEMs as a function of temperature, where E_a was calculated from the slope of the linear regression and (b) conventional conductivity *vs.* temperature.

energy for each membrane was calculated from the slope of the best-fit linear regression by plotting the natural logarithm of its ionic conductivity *versus* $1/T$ using Arrhenius eqn (1).[34]

$$\ln(\sigma_{OH^-}) = \ln(\sigma_o) - \frac{E_a}{RT} \quad (1)$$

where σ_{OH^-} is ionic conductivity, σ_o is the pre-exponential factor, R is the gas constant, and T is the absolute temperature.[34–36] The calculated activation energies are listed in Fig. 3(a). The activation energies of R-XL20-COC-2N-2.2-PE and R-XL20-COC-2N-2.3-PE are 17.5 and 15.0 kJ mol^{-1}, respectively. The E_a values of the reinforced membranes are higher than that of self-supporting membrane XL20-COC-2N-2.1 (12.6 kJ mol^{-1}), which means that the charge transport in reinforced membranes is less efficient. This increase in activation energy of the reinforced membranes can be attributed to the internal structure of the PE support layer which is non-conductive and hinders diffusion of ions within the membranes.[37,38] Even though the IEC of XL20-COC-2N-2.1 membrane is lower than those of reinforced membranes, since its entire surface area and inner structure allow ion conduction, it requires a less energy input to transport hydroxide ions.[39] The hydroxide conductivity of R-XL20-COC-2N-2.8-PE and R-XL20-COC-2N-2.5-PE samples could not be measured because these two high IEC samples showed significant curling behaviour. Overall, R-XL20-COC-2N-2.2-PE with 2.2 mequiv. g^{-1} IEC displayed the most desirable combination of properties among the reinforced membrane samples and was selected for further characterization.

2.3 Morphology

FE-SEM analysis was carried out to confirm whether the PE substrate is completely impregnated with COC anion exchange polymers with no defects. Fig. 4(a)–(c) show the surface and cross-sectional SEM images of the PE substrate, and Fig. 4(d)–(g) show the surface and cross-sectional SEM images of R-XL20-COC-2N-2.2-PE. The PE substrate (83% porosity) exhibits an opaque surface and a fibrous inner structure as shown in the surface and cross-sectional SEM images. After impregnation of COC-2N polymer solution, the PE substrate becomes transparent, as shown in Fig. 4(d). The PE substrate was densely filled with the cross-linked COC-2N polymer with no visible pores of the PE substrate and a smooth surface of top

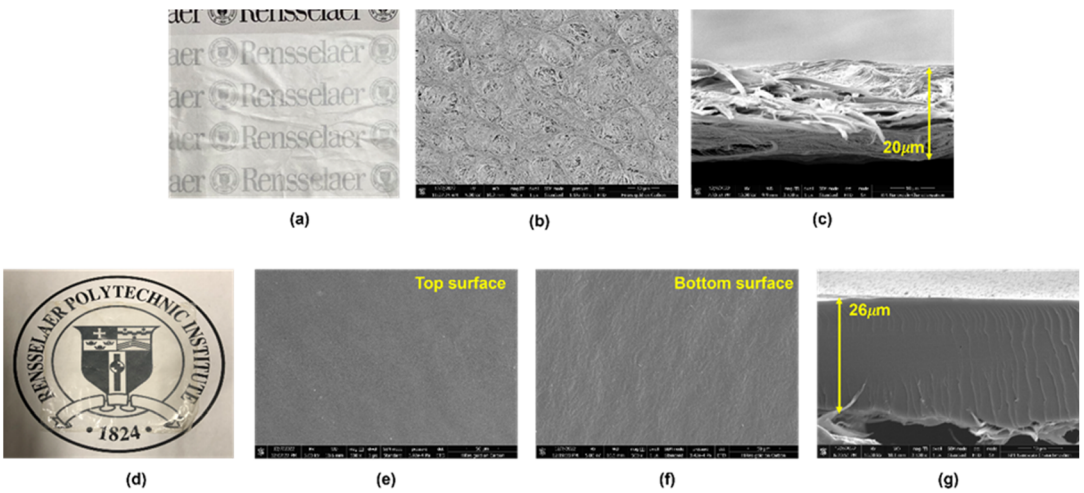

Fig. 4 (a) Optical image of the PE substrate, (b) surface and (c) cross-sectional SEM images of the PE substrate, (d) optical image of the R-XL20-COC-2N-2.2-PE membrane, and (e) and (f) surface and (g) cross-sectional SEM images of the R-XL20-COC-2N-2.2-PE membrane.

and bottom layers as demonstrated in Fig. 4(e) through (g). The total thickness of the R-XL20-COC-2N-2.2-PE membrane was approximately 26 μm. In contrast, the thickness of non-reinforced membranes should be >40 μm because we observed that when non-reinforced membranes are thinner than this value, they tend to tear easily during handling.

2.4 Mechanical properties and thermal stability

Good mechanical properties including tensile strength and elongation at break are important parameters for durability of electrolyzer applications. In this study, reinforced COC membranes were fabricated by incorporating ion-functionalized COCs into a thin, porous PE substrate to enhance membrane toughness and decrease the swelling ratio in water. The lower thickness of reinforced membranes can also contribute to decreasing membrane ohmic resistance. The stress–strain curves of the PE substrate and XL20-COC-2N-2.1 (non-reinforced, IEC = 2.1 mequiv. g^{-1}) and R-XL-COC-2N-PE membranes (reinforced, IEC = 2.2–2.8 mequiv. g^{-1}) are depicted in Fig. 5(a). The tensile strength and elongation at break of the non-reinforced XL20-COC-2N-2.1 membrane were 23 MPa and 104%, respectively. The PE substrate has weak mechanical properties (29 MPa tensile strength and 48% elongation at break) because it consists of a porous inner structure with 83% porosity. Once the pores of the PE substrate are filled with the anionic COC, the pore-filled membranes result in significantly stronger and more tough materials; the R-COC-2N-TMA-2.2-PE reinforced membrane showed a tensile strength of 49 MPa and an elongation at break of 193%. All other R-XL20-COC-2N-PE reinforced membranes with higher IECs also showed comparable mechanical properties. Due to the synergy effect of the dimensionally stable PE substrate and elastic ionic COC, the reinforced membranes showed good balance of high strength, large elongation at break, and good dimensional stability (*i.e.*, low swelling in water) while enabling a reduction in thickness. As summarized in Table S2, these reinforced COC AEMs also achieved much better mechanical properties than the state-of-the-art AEMs based on polynorbornenes. These results suggest that the impregnation of a porous PE substrate with functionalized COCs is an effective method for improving mechanical properties and reducing water swelling with a minimal impact on hydroxide conductivity.

TGA analysis was carried out to investigate thermal stability of our reinforced COC membranes. The PE substrate and non-reinforced COC AEM XL20-COC-2N-2.1 and reinforced AEM R-XL20-COC-2N-2.2-PE membranes were evaluated in a nitrogen atmosphere at a heating rate of 10 °C min from 30 to 800 °C. As shown in Fig. 5(b), the PE substrate exhibits single-step degradation at around 400 °C at which the main chain of PE was decomposed. The COC-2Br polymer undergoes a two-step degradation process; the initial degradation at 260 °C is attributed to the degradation of bromoalkyl groups on the sidechain, and the second weight loss at 400 °C is from the degradation of the COC main chain. Both the non-reinforced COC membrane and reinforced COC membrane show a three-step degradation process with temperature up to 100 °C involving loss of hydrated water and removal of residual solvents. The second weight loss between 200 and 300 °C in XL20-COC-2N-2.1 and R-XL20-COC-2N-2.2-PE was from the decomposition of QA groups on the sidechain, and the weight loss at 400 °C was due to the decomposition of the COC backbone and PE substrate. As shown in Fig. 5b, the mass change in 1st step degradation in the 200–250 °C range is slightly greater for XL20-COC-2N-2.1 (non-reinforced in the blue line) than for R-XL20-COC-2N-2.2-PE (reinforced with a PE substrate in the pink line) because the latter contains a porous polyethylene substrate in the membrane sample which starts to degrade at 400 °C.

2.5 Alkaline stability

As AEM-based electrochemical energy conversion and storage technologies operate in high pH environments, good alkaline stability of AEMs is important. We predicted that the XL20-COC-2N-2.2-PE sample would exhibit good alkaline stability due to all-carbon backbone structures of the COC and PE substrate and the absence of an aryl ether bond that is prone to suffer from degradation under alkaline conditions. The alkaline stability test was performed by soaking the XL20-COC-2N-2.2-PE sample in 1 M NaOH solution at 95 °C for 1000 hours and measuring the change in titration IEC. Fig. 6 shows the results

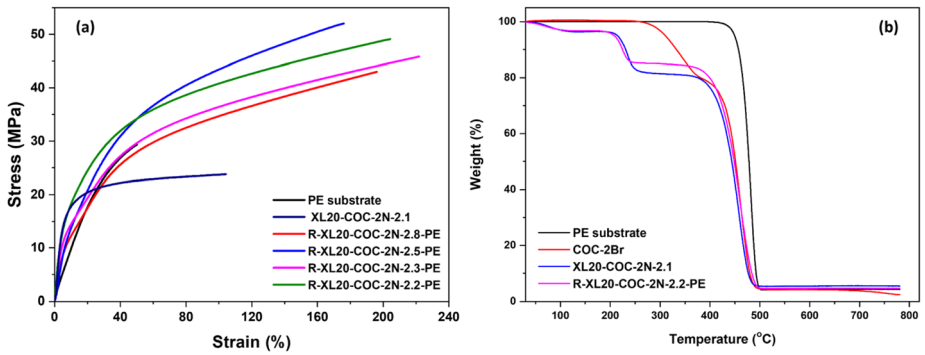

Fig. 5 (a) Tensile stress–strain curves of non-reinforced COC membranes and PE pore-filled reinforced membranes with various IECs (conditions: 50% relative humidity and 50 °C). (b) Thermogravimetric analysis data for the PE substrate, COC-2Br polymer, and XL20-COC-2N-2.1 (non-reinforced) and R-XL20-COC-2N-2.2-PE (reinforced with PE substrate) membranes.

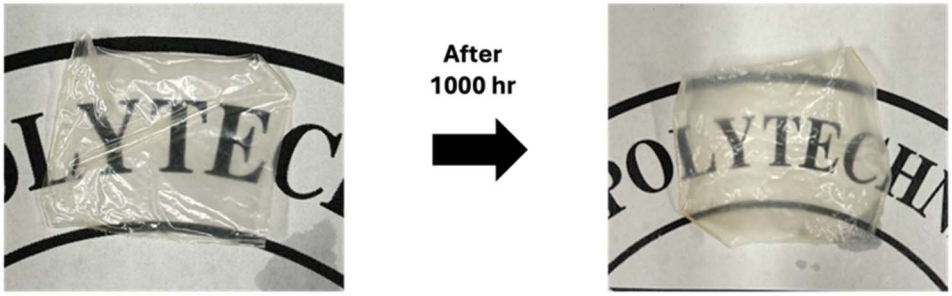

(a) R-XL20-COC-2N-2.2-PE

(b) R-XL20-COC-2N-2.2-PE after 1000 hours in 1M NaOH at 95°C

	IEC (mequiv./g)	IEC (mequiv./g) after 1,000 h	Variation in IEC
R-XL20-COC-2N-2.2-PE	2.16±0.2	2.14±0.4	-1%

Fig. 6 Alkaline stability test results of the R-XL20-COC-2N-2.2-PE membrane in 1 M NaOH solution at 95 °C for 1000 hours.

of the alkaline stability test; the measured IEC was virtually unchanged (2.16 *vs.* 2.14 mequiv. g^{-1}). When mechanical properties and Cl^- conductivity of the XL20-COC-2N-2.2-PE sample were analysed after the alkaline test, they also showed almost identical values to the pristine sample (Fig. S1 and Table S3). These results demonstrate that the XL20-COC-2N-2.2-PE sample exhibits good alkaline stability and the COC backbone and quaternary ammonium group exhibit good stability against nucleophilic attack of hydroxide ions. The membrane sample images in Fig. 6 show that before alkaline stability testing, the membrane is translucent, indicating good impregnation of the QA ionic polymer into the porous PE support. After the alkaline stability test, the membrane remained transparent. Furthermore, the reinforced AEM did not show any sign of delamination of the QA polymer from the PE support. Unfortunately, the alkaline stability test results by NMR analysis are not feasible as the prepared crosslinked membrane is insoluble.

2.6 Water electrolyzer performance and durability

Several studies have reported high-performing durable AEMs for water electrolyzers. For example, Li *et al.*[40] investigated the application of AEMs functionalized with methylpyrrolidinium cations and blended with poly(ether ketone-cardo). The electrodes comprised a NiFe layered double hydroxide on nickel felt paper as the anode and a hydrothermally synthesized MoNi alloy on nickel felt paper as the cathode. Their system demonstrated reasonable stability and conductivity, achieving a current density of 0.5 A cm^{-2} at 2 V in 1 M KOH at 60 °C with an estimated performance of 0.25 A cm^{-2} at 1.8 V. Similarly, Simari *et al.* developed composite AEMs based on quaternary ammonium polysulfone and nanoscale ionic materials for alkaline water electrolysis. The membranes were mechanically reinforced with silica-based trimethylammonium-functionalized nanoparticles to improve dimensional stability. The anode consisted of a nickel foam substrate, while the cathode employed a commercial Pt/C catalyst supported on carbon paper. The system demonstrated a current density of 3.7 A cm^{-2} at 2.2 V and 80 °C in 1 M KOH with an estimated performance of 0.81 A cm^{-2} at 1.8 V.[41] Soni *et al.*[42] developed an innovative approach for solid alkaline water electrolyzers using AEMs and ionomers based on wholly aromatic and high-molecular-weight poly(fluorene-*alt*-tetrafluorophenylene) functionalized with trimethylalkylammonium. The anode consisted of IrO_2 catalysts deposited on pressed nickel foam, while the cathode consisted of a Pt/C catalyst supported on carbon paper. Their system demonstrated a current density of 1 A cm^{-2} at approximately 1.77 V (MEA-C6) and 1.79 V (MEA-C8) in 1 M KOH at 80 °C with an estimated performance of 1.11 A cm^{-2} at 1.8 V.

Our R-XL20-COC-2N-2.2-PE membrane was evaluated in AEM water electrolyzers to determine the membrane's performance and durability in water splitting reactions. As shown in Fig. 7(a), the MEA with R-XL20-COC-2N-2.2-PE achieved a current density of 2.24 A cm^{-2} at 1.8 V, significantly outperforming the commercial PiperION AEM (40 μm, Versogen) which reached 1.50 A cm^{-2} at the same voltage. In the Nyquist plots in Fig. 7(b), the MEA with R-XL20-COC-2N-2.2-PE showed noticeably lower ohmic and charge transfer resistance than the PiperION AEM. The high ionic conductivity of the R-XL20-COC-2N-2.2-PE membrane contributed to its low ohmic resistance. Furthermore, the reinforcement with a porous PE support provides not only enhanced mechanical stability under water electrolyzer conditions but also plays a key role in reducing resistance by lowering the thickness of the membrane. These factors were crucial in achieving high performance in AEM water electrolyzers.

To assess stability of the reinforced COC AEM under device operating conditions, we conducted a durability test of R-XL20-COC-2N-2.2-PE in AEM water electrolyzer MEAs by applying a constant current of 1 A cm^{-2}. The MEA exhibited a stable voltage profile over 100 hours with a voltage decay rate of 0.13 mV h^{-1} (Fig. 7(c)), demonstrating the robustness of the membrane. A comparison of the polarization curves before and after the 100-hour durability test revealed a notable current

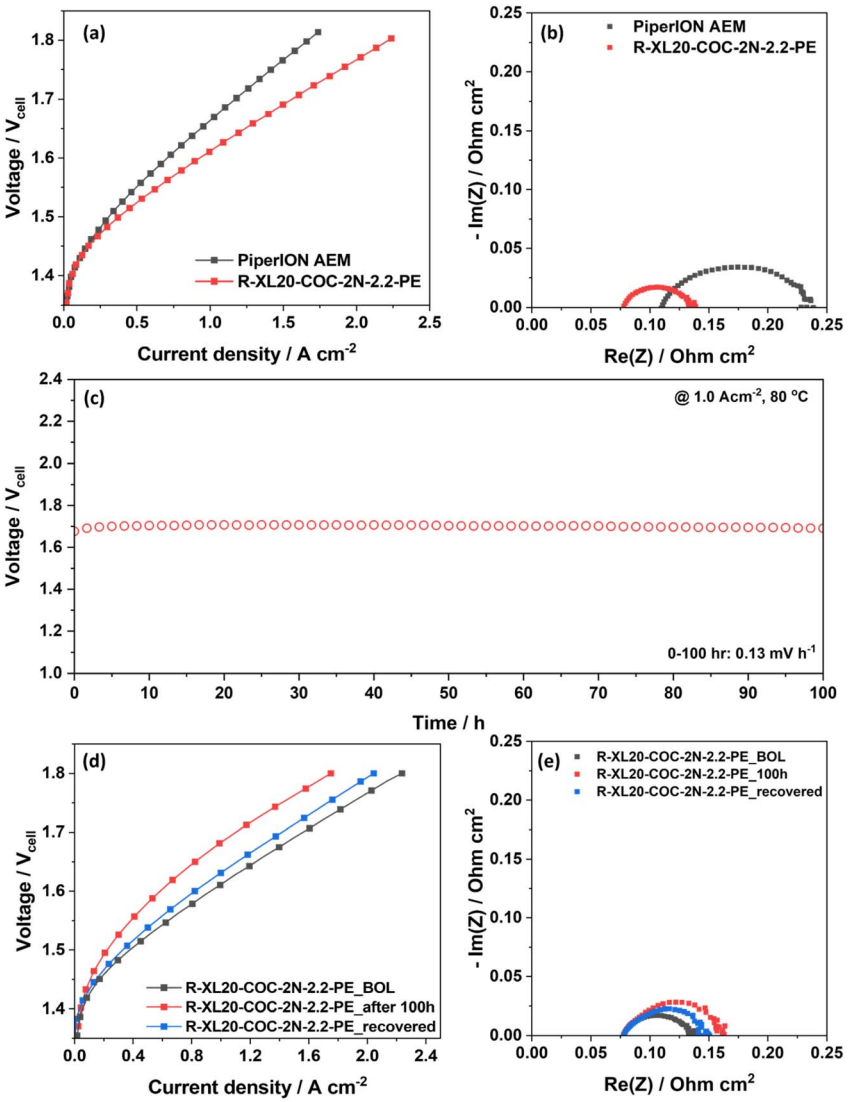

Fig. 7 Performance and durability of AEM water electrolyzers. (a) Single-cell performance comparison of R-XL20-COC-2N-2.2-PE and commercial PiperION membranes at 80 °C. (b) Nyquist plots at 1.75 V_{cell} for both electrolyzers. (c) Durability test at a constant current of 1.0 A cm^{-2} over 100 hours. (d) Polarization curves obtained after the durability test and following a 24-hour rest period. (e) Nyquist plots corresponding to the polarization curves at 1.75 V_{cell}. Details of MEA components are provided in the Experimental section.

density loss immediately following the test, which was largely recovered after a 24-hour rest period (Fig. 7(d)). This suggests that the performance loss is recoverable and likely related to bubble formation.[43] Additionally, Nyquist plots confirm that the ohmic resistance of the MEA remained unchanged after 100 hours of continuous operation, indicating good stability of the membrane in water electrolysis (Fig. 7(e)). When we compare our AEM water electrolyzer performance data with other literature results (Table S4), under similar operating conditions, our results based on reinforced COC membranes outperformed most of the state-of-the-art AEM water electrolyzers. A few reported AEM water electrolyzer systems exhibit better performance than ours due to the use of more advanced catalysts. Overall, these results underscore not only excellent membrane properties of our reinforced COC AEM but also its outstanding stability and resilience, making it a strong candidate for advanced AEM water electrolyzer systems.

3. Conclusions

In this study, quaternary ammonium-functionalized COCs that are composed of an all carbon–carbon backbone and a flexible alkyl sidechain are prepared as a low-cost, chemically stable AEM material. To reduce swelling and enhance dimensional stability in water, reinforced composite membranes are prepared by impregnating the functionalized COC into a mechanically robust polyethylene matrix. XL20-COC-2N-2.2-PE, a reinforced COC membrane with 20% crosslinking density and 2.2 mequiv. g^{-1} IEC, shows a high hydroxide conductivity of 127 mS cm^{-1} at 80 °C and low water swelling ratio of 8%. Its mechanical properties demonstrate features of

a tough material with a tensile strength of 49 MPa and an elongation at break of 205%. The reinforced COC membrane also shows good alkaline stability when evaluated in 1 M NaOH at 95 °C for 1000 h. The MEAs incorporating the R-XL20-COC-2N-2.2-PE membrane exhibited promising performance in water electrolyzers. In water electrolyzers, the MEA demonstrated exceptional performance due to its low ohmic and charge transfer resistance. Overall, our results demonstrate that the COC is a good polymer backbone choice for AEMs with the advantages of convenient scalability, low-cost synthesis, and excellent alkaline stability. Impregnation of functionalized COCs into a porous substrate yields reinforced membranes that show greatly improved mechanical properties and dimensional stability under hydrated conditions. The pore-filled reinforced composite membranes afford low ohmic resistance and good performance in AEM water electrolyzers with no sign of degradation in a 100-hour durability test. Overall, this study demonstrates that a new class of all C–C backbone based cyclic olefin copolymers and reinforced composite membranes serve as durable high-performance AEMs for water electrolyzers.

4. Experimental

4.1 Materials

Dicyclopentadiene, styrene, γ-butyrolactone, and methylaluminoxane (10% in toluene) were purchased from Sigma-Aldrich. Ethylene was acquired from Airgas. Methyl magnesium bromide Grignard reagent (3 M solution in diethyl ether), trifluoromethanesulfonic (triflic) acid, toluene, trimethylamine solution (31–35 wt% in ethanol), dichloromethane-d_2 (CD_2Cl_2), chloroform-d ($CDCl_3$), sodium chloride and sodium hydroxide were purchased from Thermo Fisher Scientific. Rac-ethylene {bis(indenyl)} zirconium(IV) dichloride ((EBI)$ZrCl_2$) and silver nitrate were purchased from Strem Chemicals. Sodium methoxide (5.4 M, 30 wt% solution in methanol) was obtained from Acro Organics. The ultra-high molecular weight polyethylene porous substrate was donated by Lydall Inc. (Solupor 3P07A, thickness = 20 μm and porosity = 83%). Sodium nitrate and hydrobromic acid were purchased from Fisher Bioreagents and Fluka, respectively. All chemicals were used without further purification.

4.2 Synthesis of functionalized cyclic olefin copolymers

To synthesize phenylnorbornene (PhNB), dicyclopentadiene, styrene, and hydroquinone were added to a glass pressure reactor and stirred at 180 °C for 6 h. After reacting for 6 h, the viscous solution was transferred to a round bottom flask with a vacuum distillation setup. PhNB was obtained at ~800 mTorr and 70–120 °C and then stored under an inert atmosphere with 4 Å molecular sieves overnight before use.

Copolymerization of PhNB and ethylene was conducted using a high-pressure reactor under inert conditions. A solution of (EBI)$ZrCl_2$ in anhydrous toluene was prepared as a polymerization catalyst and activated using MAO as a cocatalyst. PhNB in anhydrous toluene was added to a Parr reaction vessel, and then the catalyst/cocatalyst solution was injected. After that, ethylene gas was fed into the reactor at 50 psi and then stirred and heated at 70 °C for 20 min to synthesize the COC-Ph polymer. The solution was poured into methanol to precipitate the polymer, and this mixture was stirred overnight. Once COC-Ph is filtered, it is dissolved in tetrahydrofuran, filtered through a pack of alumina and precipitated by adding methanol. The collected COC-Ph was dried under vacuum at 60 °C. The PhNB unit content in COC-Ph was calculated from the ratio of aromatic peaks to alkyl peaks in the ^{1}H NMR spectrum.

To synthesize 1,7-dibromo-4-methyl-helptan-4-ol, γ-butyrolactone was added dropwise to sodium methoxide in a round-bottom flask over 1 h with stirring. After complete addition, the solution was heated to remove methanol using a vacuum distillation setup and cooled to room temperature. Once methanol was removed under vacuum, a yellow/brown solution remained in the flask. HBr was added to this yellow/brown solution dropwise at 0 °C for 1 h, and then the resulting solution was heated to 85 °C for 2 h. After solution's phase separation occurred, the organic phase (lower) was removed and the aqueous phase was washed with diethyl ether. The combined organic phase was dried with $MgSO_4$, and then the solution was evaporated to remove diethyl ether. The ketone product, 1,7-dibromohepatan-4-one, was purified by vacuum distillation. To reduce the ketone functionality to the corresponding tertiary alcohol, diethyl ether was added to the ketone and then cooled to 0 °C. Methyl magnesium bromide (3 M solution in diethyl ether) was added dropwise *via* a syringe or a syringe pump over 1 h. The reaction was allowed to warm to room temperature and then stirred for 4 h. A saturated NH_4Cl solution (50 ml) was slowly added to the reaction mixture, and then 50 ml of water was added. The organic phase was transferred to an Erlenmeyer flask, and the aqueous phase was washed three times with diethyl ether. The combined organic phase was then dried with $MgSO_4$ and evaporated to give the final product 1,7-dibromo-4-methylhaptan-4-ol.

Lastly, COC-Ph was functionalized with 1,7-dibromo-4-methylhaptan-4-ol by the Friedel–Crafts alkylation reported in our previous literature.[20] COC-Ph was dissolved in anhydrous dichloromethane and then cooled to 0 °C with an ice bath. 1,7-Dibromo-4-methylhaptan-4-ol and triflic acid were added sequentially. Once addition was completed, the solution was stirred at 0 °C and room temperature for 15 min each. The solution was poured into methanol and stirred for 1 h and then filtered. The collected COC-2Br crude product was redissolved in tetrahydrofuran and poured into methanol and filtered, giving the final product COC-2Br.

4.3 Preparation of pore-filled reinforced membranes

The procedure for preparation of reinforced COC membranes is graphically illustrated in Fig. 8. The COC-2Br polymer was dissolved in toluene at a concentration of 5 wt%, and then 20 mol% of the bromine group of COC–Br was crosslinked by adding 0.2 equivalent of *N*,*N*,*N*′,*N*′-tetramethyl-1,6-hexanediamine. Then this COC-2Br solution was filtered through a cotton filter. Pore-filled reinforced membranes were fabricated on a PE substrate using the following impregnation

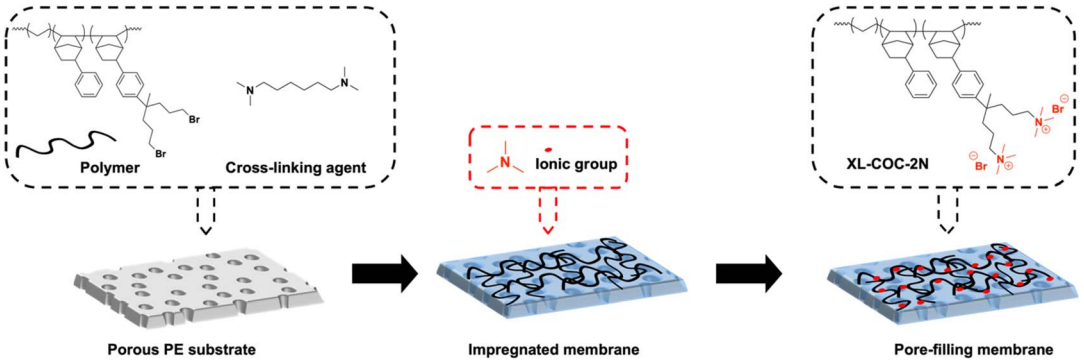

Fig. 8 Graphical illustration of pore-filled reinforced membrane preparation.

method. First, the PE substrate on top of a glass plate was submerged in toluene to wet the surface and inside pores of PE and dried at room temperature. Then the toluene solution containing COC-2Br and *N*,*N*,*N*′,*N*′-tetramethyl-1,6-hexanediamine was added dropwise to the pre-treated PE substrate and then dried at room temperature. After drying, the obtained pore-filled crosslinked COC membrane was soaked in a trimethylamine in ethanol solution for 1 day to convert the remaining terminal bromoalkyl group of the polymer to trimethylalkylammonium bromide. The pore-filled reinforced membrane was denoted as the R-XL*x*-COC-2N-*y*-PE membrane, where *x* and *y* indicate crosslinking density and IEC, respectively, and 2N indicates two QA groups per functionalized polymer unit, as shown in Fig. 8.

4.4 Membrane characterization

^{1}H NMR spectroscopy was conducted using a Varian Unity 500 MHz spectrometer using $CDCl_3$ or CD_2Cl_2 as a solvent. Weight average molecular weight (M_w) and dispersity ($Đ$) of polymers were obtained using a Viscotek GPCmax and TDA302 detector by size exclusion chromatography (SEC) using THF (0.8 ml min^{-1}) as an eluent and polystyrene standards. Thermal stability analysis of COCs, non-reinforced COC membranes, PE substrate, and reinforced COC membranes was carried out with TA Instruments TGA-Q50 at a heating rate of 10 °C min from 30 to 800 °C under an N_2 atmosphere. Mechanical properties from tensile stress–strain curves of membranes (size: 20 mm × 5 mm × 0.05 mm) were measured by dynamic mechanical analysis (DMA) using TA Instruments Q800 DMA under 50 °C and 50% relative humidity conditions with a DMA-RH accessory for the humidity-controlled experiments. A scanning electron microscope (SEM-FEI Versa 3D) was used to obtain cross-sectional and surface morphology of the porous PE substrate and COC-reinforced membranes at an accelerating voltage of 5 kV. Before measuring, all samples were coated with 60% Au and 40% Pd using a sputter coater.

4.4.1 Ion exchange capacity (IEC). IEC was calculated using NMR spectroscopy and the Mohr titration method. For reinforced COC membranes, a membrane sample in Cl^- form (approximately 100 mg) was dried at 60 °C for 2 h. The dry mass of the membrane was measured, and then it was immersed in 0.5 M $NaNO_3$ overnight. The solution was titrated with 0.1 M $AgNO_3$ using potassium chromate salt solution (K_2CrO_4) as an indicator. The IEC was calculated using the following equation:

$$\mathrm{IEC}\left(\mathrm{mmol\ g^{-1}}\right) = \frac{V_{\mathrm{AgNO_3}} \times C_{\mathrm{AgNO_3}}}{W_{\mathrm{d}}} \quad (2)$$

4.4.2 Water uptake and swelling ratio. Weight and dimensions (*x*- and *y*-directions) of a dried reinforced membrane were measured, and then it was immersed in a 1 M NaOH solution overnight to exchange counterions from Cl^- to OH^-. Then, it was soaked in water overnight to remove residual NaOH in the membrane. Once water on the membrane surface was quickly removed using a Kimwipe, its wet weight and dimensions were measured. Water uptake and the swelling ratio of reinforced membranes were calculated using eqn (3) and (4):

$$\text{water uptake } (\%) = \frac{W_{\mathrm{w}} - W_{\mathrm{d}}}{W_{\mathrm{d}}} \times 100 \quad (3)$$

$$\text{Swelling ratio } (\%) = \frac{l_{\mathrm{w}} - l_{\mathrm{d}}}{l_{\mathrm{d}}} \times 100 \quad (4)$$

4.4.3 Ionic conductivity. Hydroxide ion conductivity (σ in mS cm^{-1}) was measured using a BT-512 membrane conductivity test system (BekkTech LLC) using a four-point probe electrode method. Before measuring ionic conductivity, membrane samples with Cl^- form were changed to OH^- form by submersion in 1 M NaOH solution overnight and then rinsed with deionized water to remove excess base. Hydroxide ion conductivity was conducted in the presence of argon gas to minimize the reaction of hydroxide anion with CO_2 and prevent carbonate/bicarbonate formation. Ionic conductivity was measured at 30 °C, 60 °C, and 80 °C under fully hydrated conditions in water and it was equilibrated for at least 60 min at each temperature. Conductivity was calculated by using eqn (5):

$$\sigma\ \left(\mathrm{mS\ cm^{-1}}\right) = \frac{L}{R \times W \times T} \quad (5)$$

where L represents the distance between the two Pt wire probes (4.7 mm), R is resistance of the membrane, and W and T are the width and thickness of the membrane, respectively.

4.4.4 Alkaline stability. Reinforced membrane samples were submerged in a 1 M NaOH solution in a polypropylene container and stored at 95 °C for 1000 h. Membranes were removed from the 1 M NaOH solution at a specified time, rinsed with deionized water, and allowed to stabilize in deionized water for a minimum of 12 h before measurements (titration IEC, stress–strain, and Cl^- conductivity) were conducted.

4.4.5 Water electrolyzer assembly and testing. To evaluate the performance of the reinforced membrane for the water electrolyzer, 5 mg cm^{-2} of electrodeposited NiFe and 0.75 $mg_{PtRu}cm^{-2}$ of PtRu/C were applied to the anode and cathode, respectively. For the anode, a precursor solution was prepared by dissolving 0.04 M $Ni(NO_3)_2 \cdot 6H_2O$ and 0.01 M $Fe(NO_3)_3 \cdot 9H_2O$ in deionized water and stabilizing it overnight. Nickel foam (300 μm, Recemat BV) was cleaned *via* ethanol sonication, rinsed with DI water, and dried. Electroplating was performed at −13 mA cm^{-2} for 14 minutes in the N_2-purged solution using a three-electrode setup, with platinum mesh as the counter electrode and a hydrogen reference electrode. The plated electrode was rinsed with DI water and dried in a vacuum oven at 60 °C for 2 hours. For the cathode, the catalyst slurry, which includes 75% PtRu/C powder (50 wt% Pt, 25 wt% Ru, on HISPEC® 12100, Alfa Aesar), an ionomer (PiperION, Versogen), and IPA/H_2O solution was sprayed onto either Ni foam or carbon paper (39BB, SGL). The contents of the ionomer for the anode and cathode were 20 and 30 wt%. The catalyst-coated Ni foam and carbon paper were dried at room temperature for at least 24 h. The R-XL20-COC-2N-2.2-PE membrane was pre-treated by soaking it in 1 M KOH for 2 h, followed by rinsing with deionized water several times. It was then placed between NiFe alloy coated Ni foam and PtRu/C coated carbon paper. For comparison, a commercial PiperION AEM sample (40 μm, Versogen) was used with the same fabrication process. The active areas of both MEAs were 5 cm^2. The temperature of the single cell was maintained at 80 °C, and 1 M KOH was fed to both the anode and cathode with a flow rate of 50 ml min^{-1}. The polarization curves were obtained using the linear sweep voltage technique, increasing voltage from 1.35 to 1.8 V_{cell} with a potentiostat (SP-150e, Biologic). Using the same instrument, Nyquist plots were obtained in the frequency range from 200 kHz to 0.1 Hz at an applied voltage of 1.75 V_{cell}. An electrochemical durability test was conducted under identical temperature and feeding conditions using the same single cell. A constant current of 1 A cm^{-2} was applied for 100 hours, after which polarization curves and Nyquist plots were recorded. Following a 24-hour rest period, additional polarization curves and Nyquist plots were measured.

Author contributions

H. P.: polymer functionalization, membrane preparation and characterization, writing the original draft, writing, and editing. J. Y. J. and P. G. N.: polymer synthesis, reviewing, and editing. J. L.: membrane characterization. D. P. L. and S. Y. K.: assistance with electrolyzer performance evaluation and reviewing. Y. S. K. and C. B.: conceptualization, supervision, writing, reviewing, and editing.

Conflicts of interest

There are no conflicts to declare.

Data availability

The data supporting this article have been included as part of the supplementary information (SI). Supplementary information is available. See DOI: https://doi.org/10.1039/d5ta08898d.

Acknowledgements

The authors appreciate the financial support of the U.S. Department of Energy, Office of Efficiency and Renewable Energy (EERE), Hydrogen and Fuel Cell Technologies Office (HFCTO; with Donna Ho as program manager; DE-EE0008432), the Empire State Development Division of Science, Technology & Innovation (NYSTAR) Matching Grant Leverage Program (Contract No. C180141), and the National Research Foundation of Korea (NRF) (RS-2024-00467234 and RS-2025-02303249). Los Alamos National Laboratory (LANL) is operated by Triad National Security, LLC, under U.S. Department of Energy Contract Number 89233218CNA000001. The authors also appreciate Dr Joeseph Jang for contribution to the early experiments of this study.

Notes and references

1 G. Merle, M. Wessling and K. Nijmeijer, *J. Membr. Sci.*, 2011, **377**, 1–35.
2 S. Noh, J. Y. Jeon, S. Adhikari, Y. S. Kim and C. Bae, *Acc. Chem. Res.*, 2019, **52**, 2745–2755.
3 C. Liu, Z. Geng, X. Wang, W. Liu, Y. Wang, Q. Xia, W. Li, L. Jin and C. Zhang, *J. Energy Chem.*, 2024, **90**, 348–369.
4 M. Hren, M. Božič, D. Fakin, K. S. Kleinschek and S. Gorgieva, *Sustainable Energy Fuels*, 2021, **5**, 604–637.
5 E. J. Park, P. Jannasch, K. Miyatake, C. Bae, K. Noonan, C. Fujimoto, S. Holdcroft, J. R. Varcoe, D. Henkensmeier and M. D. Guiver, *Chem. Soc. Rev.*, 2024, **53**, 5704–5780.
6 J. R. Varcoe, P. Atanassov, D. R. Dekel, A. M. Herring, M. A. Hickner, P. A. Kohl, A. R. Kucernak, W. E. Mustain, K. Nijmeijer and K. Scott, *Energy Environ. Sci.*, 2014, **7**, 3135–3191.
7 D. R. Dekel, *J. Power Sources*, 2018, **375**, 158–169.
8 S. Gottesfeld, D. R. Dekel, M. Page, C. Bae, Y. Yan, P. Zelenay and Y. S. Kim, *J. Power Sources*, 2018, **375**, 170–184.
9 G. W. Ryoo, S. H. Park, K. C. Kwon, J. H. Kang, H. W. Jang and M. S. Kwon, *J. Energy Chem.*, 2024, **93**, 478–510.
10 M. Tanaka, K. Fukasawa, E. Nishino, S. Yamaguchi, K. Yamada, H. Tanaka, B. Bae, K. Miyatake and M. Watanabe, *J. Am. Chem. Soc.*, 2011, **133**, 10646–10654.
11 C. Fujimoto, D.-S. Kim, M. Hibbs, D. Wrobleski and Y. S. Kim, *J. Membr. Sci.*, 2012, **423**, 438–449.
12 L. Zhu, T. J. Zimudzi, Y. Wang, X. Yu, J. Pan, J. Han, D. I. Kushner, L. Zhuang and M. A. Hickner, *Macromolecules*, 2017, **50**, 2329–2337.

13 M. R. Hibbs, *J. Polym. Sci., Part B:Polym. Phys.*, 2013, **51**, 1736–1742.
14 W.-H. Lee, Y. S. Kim and C. Bae, *ACS Macro Lett.*, 2015, **4**, 814–818.
15 W.-H. Lee, E. J. Park, J. Han, D. W. Shin, Y. S. Kim and C. Bae, *ACS Macro Lett.*, 2017, **6**, 566–570.
16 C. Fujimoto, E. Sorte, N. Bell, C. Poirier, E. J. Park, S. Maurya, K.-S. Lee and Y. S. Kim, *Polymer*, 2018, **158**, 190–197.
17 M. Zhang, J. Liu, Y. Wang, L. An, M. D. Guiver and N. Li, *J. Mater. Chem. A*, 2015, **3**, 12284–12296.
18 A. Abbasi, S. Hosseini, A. Somwangthanaroj, A. A. Mohamad and S. Kheawhom, *Int. J. Mol. Sci.*, 2019, **20**, 3678.
19 J. Hao, X. Gao, Y. Jiang, H. Zhang, J. Luo, Z. Shao and B. Yi, *J. Membr. Sci.*, 2018, **551**, 66–75.
20 J. Y. Jeon, S. Park, J. Han, S. Maurya, A. D. Mohanty, D. Tian, N. Saikia, M. A. Hickner, C. Y. Ryu and M. E. Tuckerman, *Macromolecules*, 2019, **52**, 2139–2147.
21 M. Mandal, G. Huang and P. A. Kohl, *ACS Appl. Energy Mater.*, 2019, **2**, 2447–2457.
22 M. Mandal, G. Huang, N. U. Hassan, W. E. Mustain and P. A. Kohl, *J. Mater. Chem. A*, 2020, **8**, 17568–17578.
23 S. Chen, A. Zhang, X. He and D. Chen, *J. Membr. Sci.*, 2024, **700**, 122706.
24 J. C. Gaitor, A. C. Yang-Neyerlin, D. Markovich, B. P. Fors, G. W. Coates, L. F. Kourkoutis, B. S. Pivovar, T. Kowalewski and K. J. Noonan, *ACS Appl. Energy Mater.*, 2024, **7**, 1517–1526.
25 W. Chen, M. Mandal, G. Huang, X. Wu, G. He and P. A. Kohl, *ACS Appl. Energy Mater.*, 2019, **2**, 2458–2468.
26 T. Wang, Y. Wang and W. You, *J. Membr. Sci.*, 2024, **702**, 122747.
27 C. Janiak and P. G. Lassahn, *J. Mol. Catal. A:Chem.*, 2001, **166**, 193–209.
28 F. Blank and C. Janiak, *Coord. Chem. Rev.*, 2009, **253**, 827–861.
29 M. Bermeshev and P. Chapala, *Prog. Polym. Sci.*, 2018, **84**, 1–46.
30 M. Mandal, G. Huang and P. A. Kohl, *J. Membr. Sci.*, 2019, **570**, 394–402.
31 I. Tritto, L. Boggioni and D. R. Ferro, *Coord. Chem. Rev.*, 2006, **250**, 212–241.
32 X. Li and Z. Hou, *Coord. Chem. Rev.*, 2008, **252**, 1842–1869.
33 R. Jena, X. Chen, C. Yue and Y. Lam, *Polym. Test.*, 2010, **29**, 933–938.
34 M. T. Kwasny, L. Zhu, M. A. Hickner and G. N. Tew, *J. Am. Chem. Soc.*, 2018, **140**, 7961–7969.
35 D. Chen and M. A. Hickner, *Macromolecules*, 2013, **46**, 9270–9278.
36 M. L. Disabb-Miller, Y. Zha, A. J. DeCarlo, M. Pawar, G. N. Tew and M. A. Hickner, *Macromolecules*, 2013, **46**, 9279–9287.
37 M. Nilam, S. Collin, S. Karmacharya, A. Hennig and W. M. Nau, *ACS Sens.*, 2020, **6**, 175–182.
38 L. Liu, Y. Xing, Y. Li, Z. Fu, Z. Li and H. Li, *ACS Appl. Energy Mater.*, 2022, **5**, 8743–8755.
39 M. Butori, B. Eriksson, N. Nikolić, C. Lagergren, G. Lindbergh and R. W. Lindström, *Int. J. Hydrogen Energy*, 2024, **95**, 1158–1170.
40 H. Li, M. R. Kraglund, A. K. Reumert, X. Ren, D. Aili and J. Yang, *J. Mater. Chem. A*, 2019, **7**, 17914–17922.
41 C. Simari, A. Caprì, M. U. Rehman, A. Enotiadis, I. Gatto, V. Baglio and I. Nicotera, *Electrochim. Acta*, 2023, **462**, 142788.
42 R. Soni, S. Miyanishi, H. Kuroki and T. Yamaguchi, *ACS Appl. Energy Mater.*, 2020, **4**, 1053–1058.
43 A. K. Niaz, A. Akhtar, J.-Y. Park and H.-T. Lim, *J. Power Sources*, 2021, **481**, 229093.